



SPE 99462

Correlating Gel Rheology with Behavior during Extrusion through Fractures

Ying Wang and R.S. Seright, SPE, New Mexico Petroleum Recovery Research Center

Copyright 2006, Society of Petroleum Engineers

This paper was prepared for presentation at the 2006 SPE/DOE Symposium on Improved Oil Recovery held in Tulsa, Oklahoma, U.S.A., 22–26 April 2006.

This paper was selected for presentation by an SPE Program Committee following review of information contained in an abstract submitted by the author(s). Contents of the paper, as presented, have not been reviewed by the Society of Petroleum Engineers and are subject to correction by the author(s). The material, as presented, does not necessarily reflect any position of the Society of Petroleum Engineers, its officers, or members. Papers presented at SPE meetings are subject to publication review by Editorial Committees of the Society of Petroleum Engineers. Electronic reproduction, distribution, or storage of any part of this paper for commercial purposes without the written consent of the Society of Petroleum Engineers is prohibited. Permission to reproduce in print is restricted to an abstract of not more than 300 words; illustrations may not be copied. The abstract must contain conspicuous acknowledgment of where and by whom the paper was presented. Write Librarian, SPE, P.O. Box 833836, Richardson, TX 75083-3836, U.S.A., fax 01-972-952-9435.

Abstract

In many successful conformance control treatments, large volumes of gels were extruded through fractures during placement. The pressure gradient for gel extrusion depends strongly on fracture width and gel composition. Extrusion experiments directly measure gel properties in fractures, but they are both expensive and time-consuming. In this work, we investigated whether using rheology measurements to assess gel properties in fractures might prove a good substitute for the extrusion experiments, at a much more reasonable cost. The rheology behavior of the gels tested showed a strong parallel to the results obtained from previous gel extrusion experiments. However, for a given aperture (fracture width or plate-plate separation), the pressure gradients measured during the gel extrusion experiments were much higher than anticipated from rheology measurements. Extensive experiments established that wall slip and first normal stress difference were not responsible for the pressure gradient discrepancy. Steady shear and oscillatory shear data were collected with a rheometer using both smooth and rough parallel-plate geometries and employing various gap heights. Wall-slip effects were present with smooth plates but negligible with rough plates.

To explain the discrepancy, we noted that the aperture for gel flow (for mobile gel wormholing through concentrated immobile gel within the fracture) was much narrower than the width of the fracture. Considering the shear-thinning properties of the gels, two models were developed using shell momentum balances. The first model explained why the pressure gradient for gel extrusion varied inversely with the square of the fracture width rather than inversely with fracture width. In particular, the relationship depends on the power-law index of the material. The second model correlated pressure gradient, shear stress, flow rate, and shear rate to bridge the gap between gel rheology in fractures versus in a rheometer.

Introduction

Excess water production increasingly plagues oil and gas production worldwide. In naturally fractured reservoirs, large volumes of Cr(III)-acetate-HPAM gels have been successfully extruded into place to reduce channeling and excess water production.¹⁻⁴ During gel placement in fractures, the pressure gradient for gel extrusion depends strongly on fracture width and gel composition.⁵⁻⁷ Extrusion experiments directly measure gel properties in fractures, but they are both expensive (for core materials and casting) and time-consuming (two to three days per experiment, with one to two weeks of setup time). In contrast, a single rheology test can be performed at a fraction of the cost (negligible cost for gel materials) and can be completed within several minutes (after one to two days of setup time). Therefore, we investigated whether rheology testing is a more cost-effective and efficient method for predicting gel behavior in fractures.

Earlier researchers⁸⁻¹⁷ employed rheology measurements to characterize gels and gelants that are used for water shutoff. They used dynamic viscometry measurements to monitor the gelation process and study gel properties after gelation. They found that Cr(III)-acetate-HPAM gels behaved as Bingham plastics under steady shear, exhibiting a linear relationship between shear stress and shear rate above a yield stress. Bird *et al.*¹⁸ used a simple force balance to develop an equation that related yield stress to the maximum pressure drawdown that a gel could withstand.

We encountered two apparent discrepancies, however, in using rheometers to predict gel behavior in fractures. First, a simple force balance predicted that the pressure gradient required for gel extrusion between two parallel plates should be inversely proportional to the open width between the plates.¹⁸ However, when gels extruded through fractures, the pressure gradient was (roughly) inversely proportional to the square of the fracture width.^{6,19} Second, the pressure gradients observed during gel extrusion through the fractures were much greater (by more than 10 times) than those predicted by the simple force balance approach.⁵⁻⁷

We studied wall-slip effects and first normal stress differences to understand why the simple force balance underestimated the pressure gradients required for gel extrusion. We also used two models based on power-law and shell momentum balance concepts to explain the discrepancy in the relationship between pressure gradient and fracture width, and to correlate pressure gradient, shear stress, flow rate, and shear rate.

Rheology Measurements

Materials. The polymer used for all experiments was a partially hydrolyzed polyacrylamide (HPAM): Ciba Alcolflood 935™ with a molecular weight of 5×10^6 daltons and 5-10% degree of hydrolysis. Chromium acetate was used as the crosslinker. Our standard 1X, 2X, and 3X gels were used in the measurements. The 1X gel contained 0.5% Alcolflood 935 HPAM, 0.0417% Cr(III) acetate, 1% NaCl, and 0.1% CaCl_2 . The multipliers of X refer to the HPAM and chromium acetate concentrations relative to those used in our standard 1X gel. In all cases, the HPAM/Cr(III)-acetate ratio was fixed at 12:1, and the gels were aged for 24 hours at 41°C before testing.

Rheometer. Rheology measurements were performed with a Paar-Physica UDS 200™ Universal Dynamic Spectrometer fitted with a parallel-plate geometry MP 31 (50-mm diameter) for the wall-slip tests. The rheometer was equipped with a temperature control unit capable of maintaining the sample temperature at $41 \pm 0.2^\circ\text{C}$. A parallel-plate geometry was used with double-rough surfaces to eliminate wall-slip effects. A cone-plate geometry MK 22 (25-mm diameter, 1°) was used for normal stress measurements. Samples were loaded using syringes without needles.

Procedures. First, steady shear measurements with controlled shear rate (CSR) were performed using different gap heights and various rough surfaces to identify the existence of wall-slip effects and to compare the results of wall-slip prevention measures. For the first set of tests, the gap between the parallel plates was set at $h_1 = 0.5$ mm. The upper plate was rotated at a fixed shear rate and the resultant stress measurement on the bottom plate was recorded. This test was repeated for a range of shear rates to obtain the flow curve (i.e., stress versus shear rate). For the next set of tests, the gap height was increased to $h_2 = 1$ mm, and the above processes were repeated to obtain another flow curve. These procedures were performed on smooth, sandblasted, profiled, and sandpaper-covered surfaces using our 1X, 2X, and 3X gels.

Second, amplitude and frequency sweeps were performed to verify the existence of wall-slip effects and to determine the yielding area. Strain amplitude sweeps were performed at a constant frequency of 1 Hz over the strain range of 1– $10^5\%$ to obtain storage modulus (G') and loss modulus (G''). Frequency sweeps were conducted at 10% strain to ensure linear viscoelastic response over the frequency range from 0.1–10 Hz. Frequency sweep was used to compare dynamic moduli with values obtained from the amplitude sweep. These measurements were conducted on smooth, sandblasted, profiled, and sandpaper-covered surfaces with our 1X, 2X, and 3X gels.

Steady shear tests with controlled shear stress (CSS), also known as creep tests, were performed to determine yield stress. Stress was incremented stepwise from 10 to 500 Pa, depending on the different gels used, and the resultant shear rate was recorded. When shear stress was applied above the yield stress, the gels typically reached steady state in less than 10 seconds. Yield stress values were defined as the lowest points at which stress produced steady state deformation. The

time required for each step ranged from about 10 to 100 seconds.

Steady shear tests with controlled shear rate were also performed to measure first normal stress difference. Normal force (F_N) was preset as zero prior to loading the sample; the sample was then loaded and a wait period ensued until the normal force returned to the original preset value, or a stable value close to zero. The shear rate was preset to increase stepwise from 0.005 to 1000 s^{-1} , depending on the material, and the rheometer recorded the resultant first normal stress difference. The time to reach steady state ranged from about 0.1 to 100 s, depending on the shear rate: the smaller the shear rate, the longer the time required to reach steady state. Measurements of first normal stress difference were performed using our 1X, 2X, and 3X gels.

Wall Slip

Literature Review. When gel is extruded through a fracture, a minimum pressure gradient must be applied in order for the gel to flow, which suggests the gel material exhibits a yield stress.^{5-7,19} The yield point is the end of a reversible elastic deformation and the beginning of an irreversible deformation, or viscoelastic/viscous flow. In the low deformation range, the material exhibits a stable, solid-like structure which displays elastic behavior. But when the deformation exceeds the tolerance of the 3-D network, the structure is destroyed and the material flows. For a gel with yield stress, τ_y , under stationary (steady rate) conditions, Bird *et al.*¹⁸ used a simple force balance to calculate the minimum pressure gradient, dp/dl , required for gel to extrude through two parallel plates separated by a distance of w :

$$dp/dl = 2\tau_y/w \dots\dots\dots (1)$$

Employing a UDS 200 rheometer with a smooth surface, parallel-plate geometry, Liu¹⁶ estimated the yield stress of a 1X Cr(III)-acetate-HPAM gel in the range of 10 to 88 Pa. Using these values and an aperture of 1 mm (0.04 in), Eq. 1 predicted pressure gradients between 20 and 176 kPa/m (0.9 and 7.8 psi/ft). In contrast, the experimentally measured values ranged from 633 to 1,130 kPa/m (28 to 50 psi/ft) when the fracture width was 1 mm.⁷ Therefore, the yield stresses from Liu greatly underestimated the pressure gradients required for gel extrusion through fractures.

What factors might lower the measured value of yield stress? Macosko²⁰ mentioned that for viscoelastic materials, wall-slip effects were particularly prevalent during yield stress measurements. He noted that because of the impenetrability of the wall, the layer of particles adjacent to the rheometer wall was typically more dilute than the bulk dispersion. During flow, the shear rate gradient caused particles to migrate away from the wall. The thin, dilute layer near the wall had a much lower viscosity—creating the impression that the bulk fluid was slipping along the wall. Since the yield point was a flow/no-flow point as well as a transition point from elastic solid to viscous liquid, the existing thin, dilute layer acted as if the yield point had been reached and the material had already started to flow. The measured yield stress, in this case, was lower than its actual value. When measuring rheology

properties using a smooth-surface geometry, wall-slip effects could exist and diminish the measured yield stress.¹⁵⁻¹⁸ Therefore, wall-slip effects must be identified and eliminated to ensure that the measured results are properties of the gels and not artifacts produced by the method of investigation.

In our research, we used the method outlined by Yoshimura and Prud'homme^{21,22} to analyze wall-slip effects. Two assumptions were made when using this method: 1) that wall layer thickness was small compared to the viscometer gap, and 2) that slip velocity was only a function of stress once steady state was achieved. Yoshimura and Prud'homme measured stress versus shear rate with two different gap heights, h_1 and h_2 . They found that if wall slip did not exist, the sample was purely sheared and the rheometer gap size would not play any role in the measurements. On the other hand, if wall slip occurred, the apparent viscosity increased with greater gap height. As gap height increased, the thin lubricating layer that was responsible for slip became less important.

According to Yoshimura and Prud'homme, the actual (corrected) shear rate at a given stress, τ_R , is

$$\dot{\gamma}_R(\tau_R) = \frac{h_1 * \dot{\gamma}_{aR1}(\tau_R) - h_2 * \dot{\gamma}_{aR2}(\tau_R)}{h_1 - h_2}, \dots\dots\dots (2)$$

with slip velocity

$$u_s(\tau_R) = \frac{\dot{\gamma}_{aR1}(\tau_R) - \dot{\gamma}_{aR2}(\tau_R)}{2 * (\frac{1}{h_1} - \frac{1}{h_2})}, \dots\dots\dots (3)$$

and with corrected viscosity

$$\eta(\dot{\gamma}_R) = \frac{(h_1 - h_2) * \tau_R}{h_1 \dot{\gamma}_{aR1}(\tau_R) - h_2 \dot{\gamma}_{aR2}(\tau_R)}, \dots\dots\dots (4)$$

where $\dot{\gamma}_{aR1}(\tau_R)$, $\dot{\gamma}_{aR2}(\tau_R)$ are the apparent shear rates at a given shear stress.

Steady Shear Tests (CSR) for Flow Curve. Flow curves for 1X, 2X, and 3X gels using the smooth-surface rheometer at 0.5- and 1-mm gap heights were plotted (Fig. 1). All three gels were shear-thinning materials. The flow curves plotted for 1X and 2X gels clearly show higher shear stresses at the 1-mm gap height (solid squares) than those at 0.5 mm (open diamonds). The separation in the flow curves for these two gap heights suggests a wall-slip effect on the measurements. However, flow curves for the 3X gel with gap heights of 0.5 mm and 1 mm overlapped, indicating that the wall-slip effect was negligible.

The above measurements were repeated using rough surfaces to eliminate wall-slip effects. Sandpaper was used to cover both the bottom and upper plates. Flow curves for 1X and 2X gels are shown in Fig. 2 for the double-rough surfaces at two different gap heights. For the 1X and 2X gels, the flow curves were fairly close; thus, the wall-slip effects were significantly reduced by the double-rough surface. For the 3X

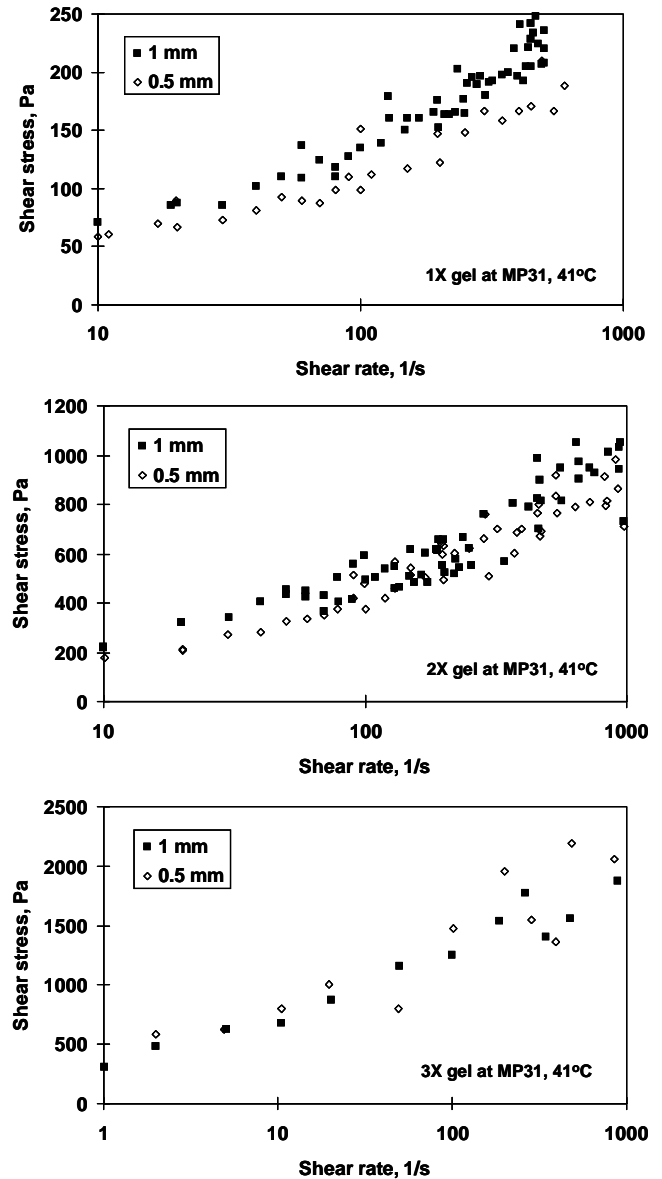


Fig. 1—Flow curves for 1X, 2X, and 3X gels on smooth surfaces.

gel, flow curves for the various surfaces were not significantly different.

Using Yoshimura and Prud'homme's method to correct for wall slip on the smooth surface, we generated corrected flow curves for the 1X and 2X gels and compared these with those for double-rough surfaces. The corrected flow curves for smooth surfaces are shown by the solid curves in Fig. 2. The corrected flow curves generally overestimated the shear stress curves at low shear rates and underestimated the shear stress values at high shear rates. More work is needed to understand this behavior.

Oscillatory Measurements. Oscillatory measurements were also performed to detect wall-slip effects and to verify the viscoelastic property of the gels. Gap heights were varied from 0.5 to 2 mm and various surfaces were employed for evaluating the presence of wall-slip effects. Fig. 3 compares storage (G') and loss (G'') moduli for a 1X gel on smooth and rough surfaces at various gap heights.

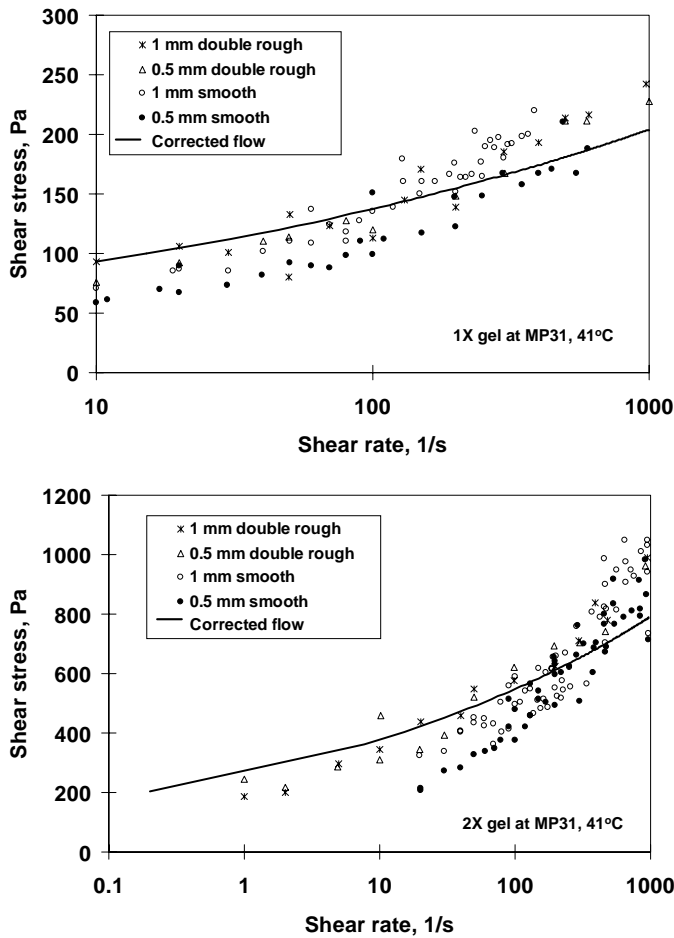


Fig. 2—Flow curve comparison of 1X and 2X gels on different surfaces.

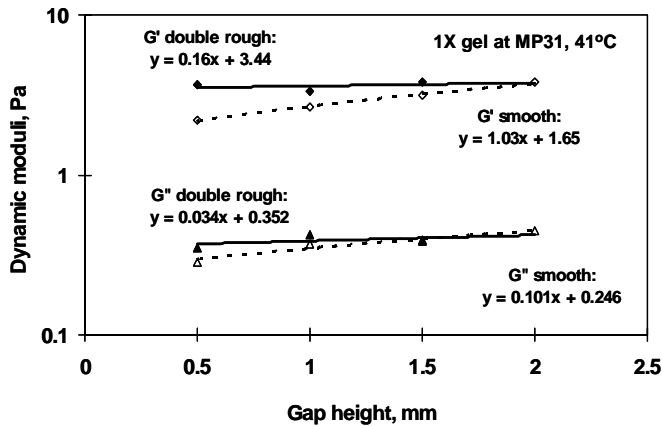


Fig. 3—Dynamic property comparison for a 1X gel versus gap on different surfaces.

This figure reveals the following points for the 1X gel: (a) on smooth surfaces, both storage and loss moduli increased with gap height, indicating the presence of wall-slip effects; (b) on double-rough surfaces, storage and loss moduli were nearly independent of gap height, indicating that the wall-slip effects were reduced by the rough surfaces; and (c) storage and loss moduli on double-rough surfaces were larger than those measured on smooth surfaces, indicating that wall-slip effects were reduced by double-rough surfaces. These

conclusions were consistent with observations from the steady shear tests. Similar studies using the 2X and 3X gels were less definitive.

Creep Tests. Creep tests were performed using the double-rough surfaces to determine yield stress (i.e., when the gels began to flow). Fig. 4 shows creep test results for our 1X, 2X, and 3X gels. The yield stress was identified when the strain-versus-time curves became sensitive to the applied stress. For example, for the 1X gel, the strain-versus-time curves were insensitive to the applied stress below 71 Pa; above 71 Pa the strain-versus-time curves were significantly higher. From Fig. 4, the yield stress was 72 Pa for the 1X gel, 141 Pa for the 2X gel, and about 400 Pa for the 3X gel. Liu^{16,17} measured the yield stress of a 1X gel by tangent crossover on the flow curve. She listed three possible values for yield stress, from 10 to 88 Pa. She had difficulty determining the actual yield point. The yield stress from our measurements on the 1X gel was closer to her highest value. The other two possible choices for yield point from Liu’s work may have been influenced by wall slip.

Table 1 summarizes the above measurements and analysis of rheology properties for our 1X, 2X, and 3X gels.

Table 1—Rheology properties of Cr(III)-acetate-HPAM gels at 41°C

Material	Yield Stress τ_y , Pa	Consistency Index k	Power Index n	Storage Modulus G' , Pa	Loss Modulus G'' , Pa
1X gel	72	41.5	-0.75	3.81	0.444
2X gel	141	219	-0.79	36.1	0.587
3X gel	400	537	-0.81	117	1.90

The consistency index and power index were obtained by fitting flow curves to the stress-versus-shear-rate values from tests with controlled shear rate (Fig. 1). The flow behavior of 1X, 2X, and 3X gels were described by the Herschel-Bulkley model²⁰ as follows:

For 1X gel: $\tau = 72 + 41.5\dot{\gamma}^{0.25}$ ($\tau > 72$ Pa)..... (5)

For 2X gel: $\tau = 141 + 219\dot{\gamma}^{0.21}$ ($\tau > 141$ Pa)..... (6)

For 3X gel: $\tau = 400 + 537\dot{\gamma}^{0.19}$ ($\tau > 400$ Pa)..... (7)

When the shear stresses were lower than the yield stress, shear rates were zero.

Using the yield stress, we calculated the pressure gradient required for gel extrusion through the fracture using the simple force balance approach. Assuming 1X gel was injected into a 1-mm wide fracture, the pressure gradient was 143 kPa/m (6.3 psi/ft). This prediction was comparable to that of Liu—still much less than the results from the extrusion experiments. The main value of this investigation was that we identified a more reliable means to determine the yield stresses for our 1X, 2X, and 3X gels. We also established that wall slip was not primarily responsible for the apparent discrepancy between rheology measurements and extrusion results in fractures.

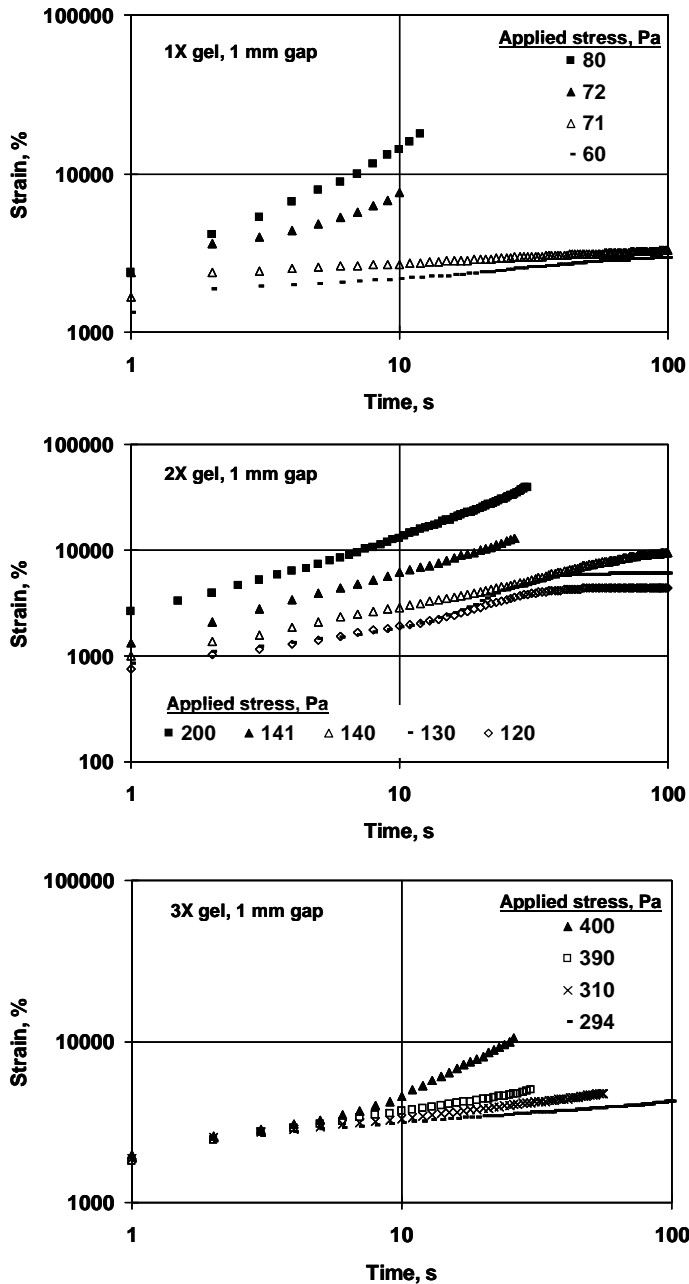


Fig. 4—Creep tests for 1X, 2X, and 3X gels on MP31, double-rough surface at 41°C.

First Normal Stress Difference

Literature Review. We wondered whether normal stress differences were responsible for the unexpectedly high pressure gradients during gel extrusion through fractures. Previous researchers studied first normal stress difference in the form of extrudate, or die swell²⁹⁻³¹ (i.e., the expansion that occurs when a viscoelastic liquid leaves a capillary die), or as the Weissenberg effect^{32,33} (i.e., during stirring, viscoelastic liquids creep up the stir shaft—also known as stir-rod climbing). In these previous studies, first normal stress difference was measured in steady shear flows^{29,34-38} or was predicted by models.^{29-31,39} For polymers, the steady shear response for the first normal stress difference, N_1 , usually

exhibits the maximum slope at low shear rates and then gradually flattens out as shear rate increases.³⁶

Both the die swell and Weissenberg effects are related to first normal stress difference. With a simple viscous fluid, only the resistance force (F) or the shear stress (τ) occurs and acts in the direction of flow, but no force acts perpendicular to the wall. With a viscoelastic material, a normal force (F_N) can occur that presses the two shearing areas apart. The normal stress (T) occurs due to anisotropic microstructures present in the viscoelastic material. When a viscoelastic material is sheared between two parallel surfaces (Fig. 5), two normal stress differences are produced in addition to the viscous shear stress; these two normal stress differences are $N_1 = T_{11} - T_{22}$ and $N_2 = T_{22} - T_{33}$. The subscripts are defined as follows: “1” is the flow direction, “2” is the direction perpendicular to the surfaces between which the fluid is sheared, and “3” is the neutral direction.

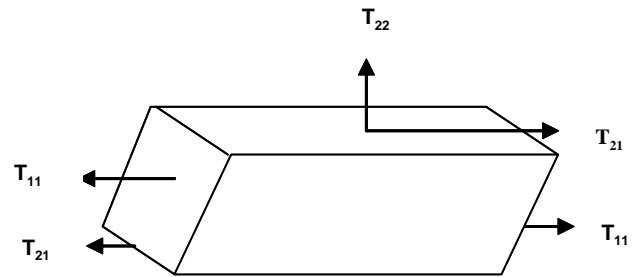


Fig. 5—Viscous shear stress and normal stresses.²⁰

The larger of the two normal stress differences is N_1 , and it is responsible for the rod-climbing phenomenon. For isotropic materials, N_1 is positive in sign (unless it is zero). In a rheometer with cone-plate geometry, N_1 causes the cone and plate surfaces to be pushed apart.

Results and Discussion. During our extrusion experiments in 1-mm wide fractures, the injection rates were between 0.046 and 23.4 cm/s, which translate to shear rates (at the wall) between 0.92 and 468 s^{-1} . We performed steady shear measurements in our rheometer to determine the first normal stress difference within this range of shear rates.

As expected for our 1X, 2X, and 3X gels, the first normal stress difference increased with shear rate for all three gels (Fig. 6). N_1 was larger for the more concentrated gels, which is reasonable since more concentrated gels have greater elasticity.

For the 1X gel, the first normal stress difference increased from 442 to 19,000 Pa when the shear rate increased from 0.2 to 1,000 s^{-1} . At shear rates below 100 s^{-1} , N_1 was proportional to the square root of shear rate, $\dot{\gamma}^{0.5}$. For shear rates between 100 and 1,000 s^{-1} , N_1 was proportional to $\dot{\gamma}^{0.25}$.

For the 2X gel, the first normal stress difference increased from 1,000 to 19,900 Pa when the shear rate increased from 0.05 to 100 s^{-1} . When the shear rate was below 0.2 s^{-1} , the slope of the N_1 curve was about 2. At higher shear rates, the first normal stress difference was fairly insensitive to shear rate.

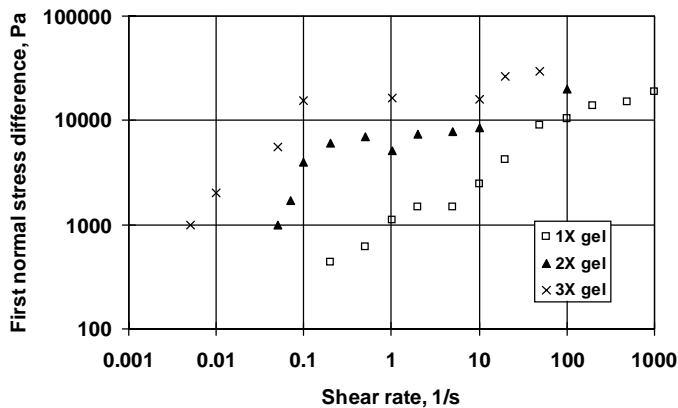


Fig. 6—First normal stress difference versus shear rate for 1X, 2X, and 3X gels at 41°C.

For the 3X gel, the first normal stress was between 1,000 and 43,200 Pa in the shear rate range from 0.005 to 60 s^{-1} . For shear rates below 0.1 s^{-1} , the slope of the N_1 curve was about 1. For shear rates between 0.1 and 100 s^{-1} , the first normal stress difference was fairly insensitive to shear rate. This behavior is qualitatively consistent with polymer behavior that was reported earlier.³⁶

The first normal stress difference depends on shear rate and flow geometry.³⁵ Therefore, for steady state flow through a fracture with smooth faces, the first normal stress difference should remain constant along the fracture. However, since fracture faces typically have rough surfaces, fracture width typically varies along the fracture length. Thus, even at the same flow rate, the shear rate could be different in different portions of the fracture. As a result, the first normal stress difference could vary along the fracture and varying pressures might be exerted on the fracture faces. Can this observation explain the difference in pressure gradient found between gel extrusion experiments in fractures and expectations from rheology measurements?

Assuming that the fracture width was 1 mm when a 1X gel was injected, the predicted pressure gradient was 143 kPa/m (6.3 psi/ft) from the simple force balance approach, compared to 633 to 1,130 kPa/m (28 to 50 psi/ft) in the extrusion experiments.^{6,7} Fig. 6 shows that the first normal stress for the 1X gel was between 442 and 19,000 Pa in the shear rate range from 0.2 to 1,000 s^{-1} . If a constriction reduced the effective fracture width by 50%, the shear rate should increase by a factor of 8 (i.e., 2^3). From Fig. 6, this variation in shear rate should not change the normal stress by more than a factor of four for the 1X gel. If normal stress is reduced from 10,000 Pa to 2,500 Pa when passing through a constriction, a pressure change of 7,500 Pa (1.1 psi) might be experienced. If 20 such constrictions were encountered along the fracture, this behavior could explain the higher pressure gradients observed during gel extrusion through fractures. However, during our extrusion experiments, we generally used fractures that did not have pronounced constrictions. More importantly, we often used fractures with smooth faces, and the pressure gradients during extrusion of a 1X gel through a 1-mm wide fracture were still from 633 to 1,130 kPa/m (28 to 50 psi/ft).^{6,7} Thus, although normal forces could add significantly to the pressure gradients observed when using fractures with many

pronounced constrictions, they do not explain the high pressure gradients observed during the bulk of our gel extrusion experiments.

Gel Dehydration and Wormholes in Fractures

Before gelation, fluid gelant solutions can readily leak off from fractures into porous rock. However, after gelation, the crosslinked materials will not penetrate significantly into the porous rock.⁵⁻⁷ Thus, formed gels must extrude through fractures during the placement process. Cr(III)-acetate-HPAM gels (as well as other gels) concentrate or lose water during extrusion through fractures. As water leaks off from the gel, the gel concentrates (by factors up to 50) to become immobile in the vicinity where dehydration occurs. The driving force for gel dehydration (and water leakoff) is the pressure difference between the fracture and the adjacent porous rock. Because fresh gel (i.e., mobile gel, with the original composition) is much more pliable and mobile than the concentrated gel, the fresh gel wormholes through the concentrated gel in order to advance the gel front.⁵⁻⁷ These wormholes may be significantly narrower than the fracture width. This possibility could explain the relatively high pressure gradients during gel extrusion.

By inputting a pressure gradient of 633 kPa/m (28 psi/ft) and a yield stress of 35 Pa (0.005 psi) (from Liu^{16,17}) into a simple force balance, Seright⁷ estimated the actual opening width to be about 0.1 mm—one-tenth of the fracture width. Similarly, using a pressure gradient range of 633 to 1,130 kPa/m (28 to 50 psi/ft) with our measured yield stress value of 72 Pa (0.01 psi), the calculated apertures were from 0.13 to 0.23 mm. Thus, the relatively high pressure gradients during gel extrusion through fractures may have resulted because the actual gel flow path (i.e., through wormholes) was significantly narrower than the fracture width.

Pressure Gradient versus Fracture Width

Literature Review. A force balance¹⁸ suggested that the minimum pressure gradients required for gel extrusion through fractures should be inversely proportional to fracture width or capillary radius. In a capillary of radius, R ,

$$dp/dl = 2\tau_y / R \dots\dots\dots (8)$$

Ganguly *et al.*²³ demonstrated that rupture pressure was inversely proportional to the inside diameter of the tube when gels (0.75% Alcoflood 935, 0.0417% Cr(III) acetate, 1% NaCl; gel time = 12 hours, gelant aged 6 to 8 days) were placed in various lengths of nylon and polypropylene tubes with different inside diameters. Seright¹⁹ noted similar results when studying failure of the 1X gel in tubes made of stainless steel, Teflon, glass, and polyetheretherketone. A power regression on the data confirmed that the failure pressure gradient was inversely proportional to the tube diameter. However, the correlation coefficient for the regression was only 0.6.

Seright⁵⁻⁷ also noted that the pressure gradient required for gel extrusion was inversely proportional to the square of the fracture width (Fig. 7). For our 1X Cr(III)-acetate-HPAM gel, the required pressure gradient (dp/dl , in psi/ft) could be

estimated using Eq. 9 (if fracture width, w_f , is expressed in inches):

$$dp/dl = 0.02/(w_f)^2 \dots\dots\dots (9)$$

We wondered why the pressure gradient required for gel extrusion through an open channel was inversely proportional to the channel width for the simple force balance approach, but was inversely proportional to the square of the fracture width in the extrusion experiments.

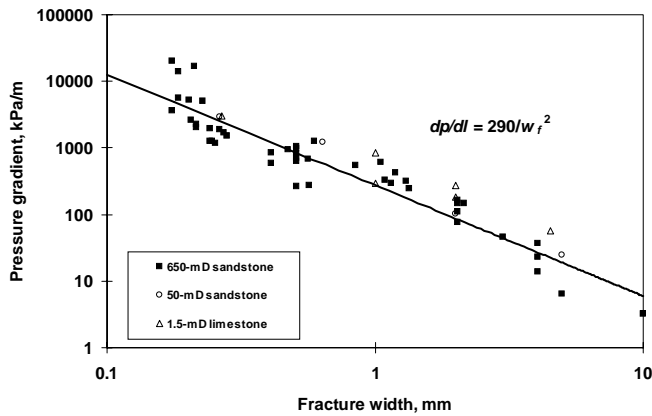


Fig. 7—Pressure gradients required for gel extrusion.⁵

To describe gel behavior in the fracture, Seright⁵ examined a Bingham model for extrusion of the Cr(III)-acetate-HPAM gels through fractures. In this model, a Newtonian fluid near the fracture wall lubricated the flow of the solid-like materials in the middle of the path. Water leaving the gel during the dehydration process could comprise the lubricating layer. The thickness of the lubricating layer should be small relative to the fracture width and increase linearly with fluid velocity.

Two flaws existed with the Bingham model. First, the pressure gradients predicted by this model should depend on the viscosity of the lubricating fluid—water in this case. Since the viscosity of water decreased by a factor of about three as temperature increased from 20° to 80°C, the measured pressure gradients for gel extrusion should also have decreased by roughly a factor of three. In reality, the pressure gradient was insensitive to temperature over this range. Second, the lubrication layer should have become thicker with increased flow rate. With a thicker lubrication layer (i.e., more water), the leakoff rate should have increased with the increased extrusion rate. Instead, the leakoff rate was independent of flow rate—it was primarily time-dependent.^{5,6}

In view of the above deficiencies, we considered an alternative model that was based on the Herschel-Bulkley model,²⁰ where the fluid exhibited a yield stress and flowed as a power-law fluid above the yield point. We employed a shell momentum balance²⁵ and power-law equations to deduce these models.

Model Based on Shell Momentum Balance and Power-Law. For steady-state flow, a momentum balance for a shell of finite thickness was first applied. As the thickness approached zero, the corresponding differential equation describing the momentum flux distribution was obtained.

Next, the appropriate Newtonian or non-Newtonian expression for the momentum flux was inserted to obtain a differential equation for the velocity distribution. Integration of these two differential equations yielded the momentum flux and the velocity distributions for the system. This information can then be used to calculate various other quantities, such as average velocity, maximum velocity, volumetric flow rate, pressure drop, and forces on boundaries.

For fluid flow inside a tube,²⁵

$$\tau = \frac{p_0 - p_L}{2L} R, \dots\dots\dots (10)$$

where R is the radius and L is the length of the tube, and p_0 and p_L are the inlet and outlet pressures, respectively. For Newtonian materials,

$$\tau = -\eta \frac{d\gamma}{dt}, \dots\dots\dots (11)$$

where τ is the shear stress, η is the Newtonian viscosity, γ is shear strain, and t is time.

Combining Eqs. 10 and 11, the velocity distribution along the radial direction is

$$v = -\frac{p_0 - p_L}{4\eta L} R^2 \left[\left(\frac{r}{R} \right)^2 - 1 \right], \dots\dots\dots (12)$$

where v is the velocity and r is the distance from the tube center.

Integrating Eq. 12, the volumetric flow rate is

$$q = \frac{\pi(p_0 - p_L)R^4}{8\eta L} \dots\dots\dots (13)$$

The pressure gradient versus tube radius is

$$\frac{dp}{dl} = 8\eta \frac{q}{\pi R^4} \dots\dots\dots (14)$$

Thus, for Newtonian materials, the pressure gradient varied inversely with the fourth power of tube radius.

For non-Newtonian materials, the power-law is

$$\tau = -k \left(\frac{dv}{dt} \right)^{n+1}, \dots\dots\dots (15)$$

where k is the consistency index and n is the power index.

The velocity distribution along the tube radius is

$$v = \left(-\frac{p_0 - p_L}{2kL} \right)^{\frac{1}{n+1}} \frac{n+1}{n+2} \left(r^{\frac{n+2}{n+1}} - R^{\frac{n+2}{n+1}} \right), \dots\dots\dots (16)$$

and the volumetric flow rate is

$$q = \left(-\frac{p_0 - p_L}{2kL} \right)^{\frac{1}{n+1}} \pi \left(-\frac{n+1}{3n+4} \right) R^{\frac{3n+4}{n+1}} \dots\dots\dots (17)$$

The pressure gradient versus tube radius is

$$\frac{dp}{dl} = (-2k) \left(-\frac{3n+4}{n+1} \right)^{n+1} \left(\frac{q}{\pi} \right)^{n+1} \frac{1}{R^{3n+4}} \dots\dots\dots (18)$$

Therefore, the pressure gradient varied inversely with the tube radius raised to the power, 3n+4, for power-law, non-Newtonian materials.

For fluids flowing between two parallel plates, the shell momentum balance reveals that

$$\tau = \left(\frac{p_0 - p_L}{L} \right) x, \dots\dots\dots (19)$$

where *x* is the distance from the center of the fracture to the fracture wall.

Following the same procedures used for tubes, for Newtonian materials, the velocity distribution along the fracture width (*w*) is

$$v_z = -\frac{p_0 - p_L}{2\eta L} w^2 \left[\left(\frac{x}{w} \right)^2 - \frac{1}{4} \right] \dots\dots\dots (20)$$

The volumetric flow rate is

$$q = \frac{1}{12} \frac{(p_0 - p_L)}{\eta L} h w^3, \dots\dots\dots (21)$$

where *h* is the fracture height and *L* is the fracture length.

The pressure gradient versus fracture width is

$$\frac{dp}{dl} = \frac{12\eta q}{h} \frac{1}{w^3} \dots\dots\dots (22)$$

Therefore, the pressure gradient varied inversely with the third power of fracture width for Newtonian materials.

For non-Newtonian materials following the power-law, the velocity distribution along the fracture width is

$$v = \left(-\frac{p_0 - p_L}{kL} \right)^{\frac{1}{n+1}} \frac{n+1}{n+2} \left(\frac{w}{2} \right)^{\frac{n+2}{n+1}} \left[\left(\frac{2x}{w} \right)^{\frac{n+2}{n+1}} - 1 \right], \dots\dots (23)$$

and the volumetric flow rate is

$$q = \left(-\frac{p_0 - p_L}{2kL} \right)^{\frac{1}{n+1}} \frac{h}{2} \left(-\frac{n+1}{2n+3} \right) w^{\frac{2n+3}{n+1}} \dots\dots\dots (24)$$

The pressure gradient versus fracture width is

$$\frac{dp}{dl} = (-2k) \left(-\frac{2n+3}{n+1} \right)^{n+1} \left(\frac{2q}{h} \right)^{n+1} \frac{1}{w^{2n+3}} \dots\dots\dots (25)$$

Therefore, for power-law, non-Newtonian materials, the pressure gradient varied inversely with the fracture width, raised to the power, 2n+3.

Summarizing the above equations, the pressure gradients required for Newtonian materials to extrude varied inversely with the fourth power of tube radius and with the third power of fracture width. For power-law, non-Newtonian materials, the pressure gradients varied inversely with tube radius raised to the power, 3n+4, and with fracture width raised to the power, 2n+3.

The relationship of pressure gradient versus tube radius/fracture width for our 1X, 2X, and 3X gels is summarized in **Table 2**. For the gels listed in this table, *q* must have units of m³/s; *R*, *w*, and *h* must have units of m; *η* must have units of Pa-s; and the calculated pressure gradients, *dp/dl*, must have units of Pa/m.

Table 2—Pressure gradient versus tube radius/fracture width for Cr(III)-acetate-HPAM gels

Material	Tube	Fracture
Newtonian	$8\eta \frac{q}{\pi R^4}$	$\frac{12\eta q}{h} \frac{1}{w^3}$
1X gel	$101q^{0.26} \frac{1}{R^{1.78}}$	$156 \left(\frac{q}{h} \right)^{0.26} \frac{1}{w^{1.52}}$
2X gel	$532q^{0.21} \frac{1}{R^{1.63}}$	$760 \left(\frac{q}{h} \right)^{0.21} \frac{1}{w^{1.42}}$
3X gel	$1300q^{0.19} \frac{1}{R^{1.57}}$	$1796 \left(\frac{q}{h} \right)^{0.19} \frac{1}{w^{1.38}}$

During extrusion experiments, Seright⁵⁻⁷ noted that the pressure gradient varied inversely with the square of the fracture width. In examining the gel entries for Table 2, the exponents ranged from 1.38 to 1.78 for the *R* variables and from 1.38 to 1.52 for the *w* variables. These exponents were intermediate between the exponent of one (predicted from a force balance with Newtonian fluids) and two (the approximate value observed experimentally).

Pressure gradients versus fracture width were plotted (**Fig. 8**) for the 1X gel flowing through fractures at a fixed volumetric rate of 16,000 ml/hr. The pressure gradient values estimated by the models were greater than those from the simple force balance approach. For aperture widths less than 2.54 mm (0.1 in), the model's calculated pressure gradients more closely matched the extrusion data than calculations from the simple force balance approach. The model described the relation between pressure gradient and aperture size fairly well as long as the aperture was not too wide (e.g., not greater than 2.54 mm).

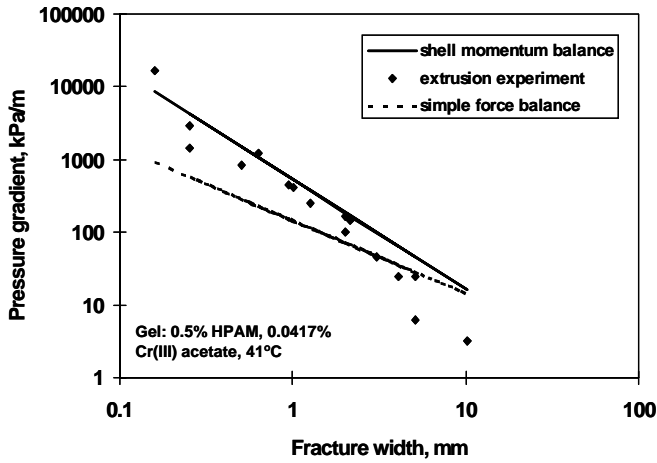


Fig. 8—Comparison of pressure gradients versus aperture for 1X gel.

We also calculated the velocity distribution versus aperture for the 1X, 2X, and 3X gels flowing through a 38.1-mm high by 1-mm wide fracture, and a tube with inside diameter of 2 mm with a flow rate of 16,000 ml/hr. Fig. 9 indicates that the gels moved more like a piston through the apertures than did the Newtonian fluid.

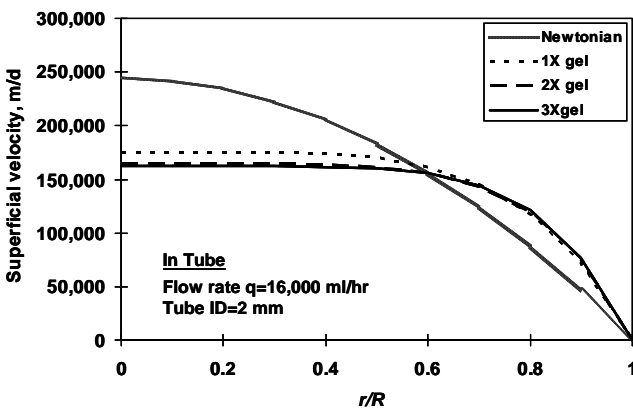
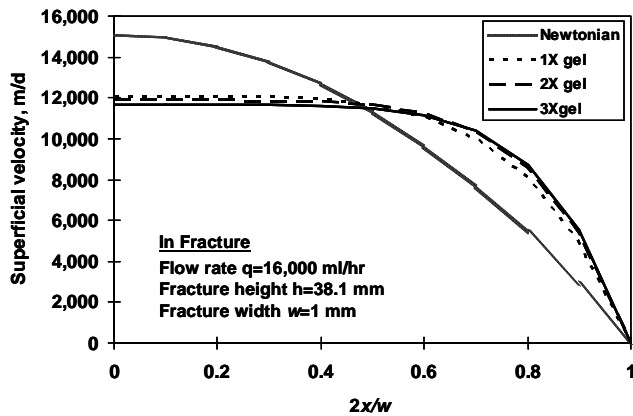


Fig. 9—Velocity distribution for 1X, 2X, and 3X gels.

Similar Relationships between Pressure Gradient versus Flow Rate and Shear Stress versus Shear Rate. During steady shear measurements, Liu^{16,17} found that for the 1X Cr(III)-acetate-HPAM gel, shear stress was fairly insensitive to shear rate (Fig. 10). When the shear rate was increased by a

factor of 10^5 , the shear stress increased only by a factor of 10. This result was consistent with Seright's findings that the pressure gradient required to extrude gel through a fracture was fairly insensitive to injection velocity. A log-log plot of complex viscosity versus shear rate gave a slope of -0.8 , which was close to the slopes (-0.83 to -0.95) for a log-log plot of resistance factor (apparent viscosity relative to water) versus injection velocity that were noted during gel extrusion through fractures.^{26,27}

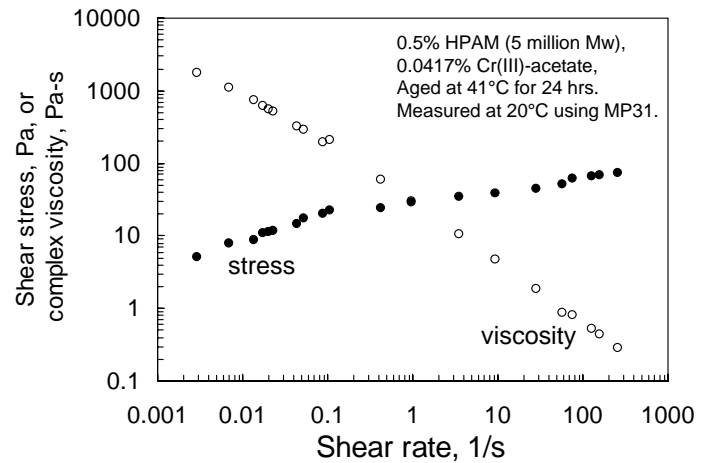


Fig. 10—Stress and complex viscosity versus shear rate.¹⁶

This interesting similarity made us consider the relationship of gel behavior in fractures versus in a rheometer. Combining Eqs. 10, 11, and 13, relate shear rate to the flow rate for Newtonian fluids in tubes:

$$\dot{\gamma} = -\frac{4q}{\pi R^4} r \dots\dots\dots (26)$$

Combining Eqs. 10, 16, and 18, give the shear rate for power-law, non-Newtonian materials in tubes:

$$\dot{\gamma} = -\frac{3n+4}{n+1} \frac{q}{\pi} R^{-\frac{3n+4}{n+1}} r^{\frac{1}{n+1}} \dots\dots\dots (27)$$

Combining Eqs. 11, 20, and 22, give the shear rate for Newtonian materials in fractures:

$$\dot{\gamma} = -\frac{12q}{hw^3} x \dots\dots\dots (28)$$

Combining Eqs. 16, 20, and 25, give the shear rate for power-law, non-Newtonian materials in fractures:

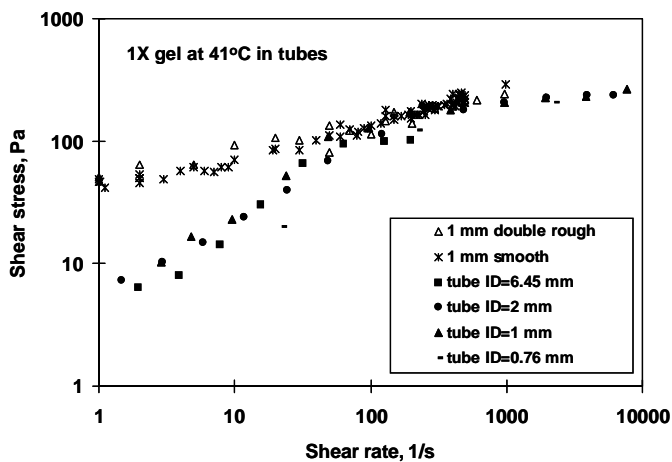
$$\dot{\gamma} = -\frac{2n+3}{n+1} \frac{2q}{h} w^{-\frac{2n+3}{n+1}} (2x)^{\frac{1}{n+1}} \dots\dots\dots (29)$$

Table 3 shows the correlations of pressure gradient, shear stress, flow rate, and shear rate at the wall, where $r=R$ or $x=w/2$, for the 1X, 2X, and 3X gels.

Table 3—Correlation of pressure gradient, shear stress, flow rate, and shear rate at the wall

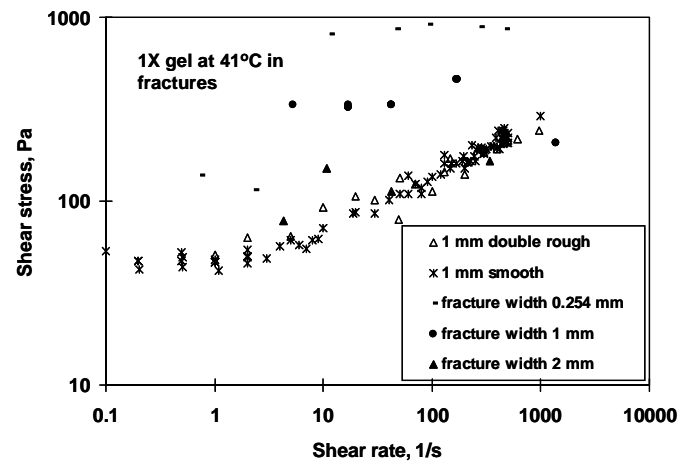
Material	Tube	Fracture
1X gel	$\dot{\gamma} = -6.93 \frac{q}{\pi R^3}$, $\tau = \frac{p_0 - p_L}{L} \frac{R}{2}$	$\dot{\gamma} = -11.86 \frac{q}{hw^2}$, $\tau = \frac{p_0 - p_L}{L} \frac{w}{2}$
2X gel	$\dot{\gamma} = -7.69 \frac{q}{\pi R^3}$, $\tau = \frac{p_0 - p_L}{L} \frac{R}{2}$	$\dot{\gamma} = -13.38 \frac{q}{hw^2}$, $\tau = \frac{p_0 - p_L}{L} \frac{w}{2}$
3X gel	$\dot{\gamma} = -8.14 \frac{q}{\pi R^3}$, $\tau = \frac{p_0 - p_L}{L} \frac{R}{2}$	$\dot{\gamma} = -14.28 \frac{q}{hw^2}$, $\tau = \frac{p_0 - p_L}{L} \frac{w}{2}$

Comparison in Tubes. Based on pressure gradients and flow rates from the extrusion experiments, we calculated shear stresses and shear rates for the 1X, 2X, and 3X gels using the equations in Table 3. These calculations were compared to the rheology measurements made with a gap height of 1 mm on smooth and rough surfaces. In tubes (Fig. 11 for the case of a 1X gel), the calculated shear-stress versus shear-rate relation followed the same trend as the rheology measurements for shear rates above 100 s⁻¹. However, the measured shear stresses were higher than the calculated values for tube flow for shear rates below 100 s⁻¹. More work is needed to understand this behavior.

**Fig. 11—Comparison of shear stress versus shear rate for 1X gel in tubes.**

Comparison in Fractures. For a 2-mm wide fracture (Fig. 12 for the case of a 1X gel), the calculated shear-stress versus shear-rate relation followed the same trend as the rheology measurements. However, for narrower fractures (0.254 mm and 1 mm), shear stress values calculated from the extrusion experiments were generally much higher than the rheology measurements. The highest shear stress values were noted in

the narrowest fracture. This discrepancy could be explained by the fairly rough Berea sandstone surface seriously interfering with gel flow in the fracture, especially for very narrow fractures. For wider fractures (e.g., 2 mm) this interference became negligible; thus, the flow curve was similar to our rheology measurements. The similarity between the flow curves from the fracture flow or tube flow and the rheology measurements helps to bridge the gap between gel behaviors in fractures or tubes with those seen in a rheometer. However, additional work is needed to fully explain the high pressure gradients observed during gel extrusion through narrow fractures.

**Fig. 12—Comparison of shear stress versus shear rate for 1X gel in fractures.**

Conclusions

When evaluating the use of gels for conformance improvement in treating channeling through fractures, rheology measurements can be made much faster and with much lower cost than measurements made during extrusion of gels through fractured cores. However, the pressure gradient required to extrude a gel through a fracture is usually substantially greater than anticipated based on rheology measurements combined with a simple force balance. This paper examined this discrepancy, in hopes of ultimately substituting the rheology measurements for extrusion experiments. The following conclusions were reached, based on studies of Cr(III)-acetate-HPAM gels at 41°C.

1. Use of double-rough, parallel plates in our rheometer significantly reduced the importance of wall slip (compared to smooth plates). However, the higher stresses noted during the absence of slip effects were not enough to explain the high pressure gradients during gel extrusion experiments.
2. Consistent with expectations, the first normal stress difference increased with shear rate and polymer concentration for our Cr(III)-acetate-HPAM gels. Although first normal stress might result in greater pressure gradients during extrusion through fractures with significant constrictions, it was not great enough to explain the high pressure gradients during extrusion experiments.

3. Earlier work revealed that gels propagate through fractures by wormholing through immobile concentrated (dehydrated) gel. Since these wormholes are narrower than the fracture width, this could partly explain the higher pressure gradients during gel extrusion experiments.
4. A model based on power-law and shell momentum balance predicted that pressure gradient should vary with fracture width raised to a power between -1 and -2 . This model fit our extrusion data reasonably well for fracture widths of 1 mm or less.
5. In 2-mm wide fractures, a second model did well in correlating pressure gradient with shear stress and flow rate with shear rate. However, in narrower fractures, the model was notably less successful. Additional work is needed to fully explain the high pressure gradients observed during gel extrusion through narrow fractures.

Acknowledgments

Financial support for this work is gratefully acknowledged from the United States Department of Energy (NETL), the State of New Mexico, ConocoPhillips, ExxonMobil, and Marathon. We greatly appreciate the effort by Annette Carroll and Julie Ruff in editing this paper.

Nomenclature

F = force, N
 F_N = normal force, N
 G' = storage modulus, Pa
 G'' = loss modulus, Pa
 h = gap height or fracture height, m
 k = consistency index
 L = fracture or tube length, m
 N = normal stress difference, Pa
 N_I = larger of two normal stress differences, Pa
 n = power index
 p_L = outlet pressure, Pa
 p_0 = inlet pressure, Pa
 dp/dl = pressure gradient, psi/ft [Pa/m]
 q = volume rate of flow, m³/s
 R = tube radius, mm
 r = radius to tube wall, mm
 T = normal stress, Pa
 U_R = slip velocity, m/s
 v = superficial velocity, m/s
 w = aperture/fracture width, mm
 w_f = fracture width, mm
 x = distance to the fracture wall, mm
 γ = shear strain, %
 $\dot{\gamma}$ = shear rate, s⁻¹
 $\dot{\gamma}_{aR}$ = apparent shear rate, s⁻¹
 $\dot{\gamma}_R$ = corrected shear rate, s⁻¹
 η = viscosity, Pa-s
 $\eta(\dot{\gamma}_R)$ = corrected viscosity, Pa-s
 τ = shear stress, Pa
 τ_R = corrected shear stress, Pa
 τ_y = yield stress, Pa

References

1. Sydansk, R.D. and Moore, P.E.: "Gel Conformance Treatments Increase Oil Production in Wyoming," *Oil & Gas J.* (January 1992) 40.
2. Borling, D.C.: "Injection Conformance Control Case Histories Using Gels at the Wertz Field CO₂ Tertiary Flood in Wyoming," paper SPE 27825 presented at the 1994 SPE/DOE Symposium on Improved Oil Recovery, Tulsa, Oklahoma, 17–20 April.
3. Hild, G.P. and Wackowski, R.K.: "Reservoir Polymer Gel Treatments To Improve Miscible CO₂ Flood," *SPEE* (April 1999) 196.
4. Lane, R.H. and Sanders, G.S.: "Water Shutoff through Fullbore Placement of Polymer Gel in Faulted and in Hydraulically Fractured Producers of the Prudhoe Bay Field," paper SPE 29475 presented at the 1995 SPE Production Operations Symposium, Oklahoma City, Oklahoma, 2–4 April.
5. Seright, R.S.: "An Alternative View of Filter Cake Formation in Fractures Inspired by Cr(III)-Acetate-HPAM Gel Extrusion," *SPEPF* (February 2003) 65.
6. Seright, R.S.: "Gel Propagation through Fractures," *SPEPF* (November 2001) 225.
7. Seright, R.S.: "Mechanism for Gel Propagation through Fractures," paper SPE 55628 presented at the 1999 SPE Rocky Mountain Regional Meeting, Gillette, Wyoming, 15–18 May.
8. Prud'homme, R.K. *et al.*: "Rheological Monitoring of the Formation of Polyacrylamide/Cr³⁺ Gels," *SPEJ* (October 1983) 804.
9. Prud'homme, R.K. and Uhl, J.T.: "Kinetics of Polymer/Metal-Ion Gelation," paper SPE/DOE 12640 presented at the 1984 AIME SPE/DOE Symposium on Enhanced Oil Recovery, Tulsa, Oklahoma, 15–18 April.
10. Pearson, D.S. and Graessley, W.W.: "The Structure of Rubber Networks with Multifunctional Junctions," *Macromolecules* (1978) **11**, No. 3, 528.
11. Aslam, S., Vossoughi, S., and Willhite, G.P.: "Viscometric Measurement of Chromium (III)-Polyacrylamide Gels by Weissenberg Rheogoniometer," paper SPE 12639 presented at the 1984 AIME SPE/DOE Symposium on Enhanced Oil Recovery, Tulsa, Oklahoma, 15–18 April.
12. Thurston, G.B., Ozon, P.M., and Pope, G.A.: "Viscoelasticity and Gelation of Some Polyacrylamide and Xanthan Gum Solutions," paper No. 62B presented at the American Institute of Chemical Engineers 1985 Spring National Meeting and Petro Expo '85, Houston, Texas, 24–28 March.
13. Kakadjian, S., Raueo, O., and Mejias, F.: "Dynamic Rheology as a Method to Quantify Gel Strength of Water Shutoff Systems," paper SPE 50751 presented at the 1999 International Symposium on Oilfield Chemistry, Houston, Texas, 16–19 February.
14. Allain, C. and Salome, L.: "Gelation of Semidilute Polymer Solutions by Ion Complexation: Critical Behavior of the Rheological Properties versus Cross-Link Concentration," *Macromolecules* (1990) **23**, No. 4, 981.
15. Broseta, D. *et al.*: "Rheological Screening of Low-Molecular-Weight Polyacrylamide/Chromium (III) Acetate Water Shutoff Gels," paper SPE 59319 presented at the 2000 SPE/DOE Symposium on Improved Oil Recovery, Tulsa, Oklahoma, 3–5 April.
16. Liu, J., and Seright, R.S.: "Rheology of Gels Used for Conformance Control in Fractures," *SPEJ* (June 2001) 120.
17. Liu, J.: "Rheological Properties of Gels Used for Conformance Control," Master Degree thesis, New Mexico Institute of Mining and Technology, Socorro, New Mexico (1999), 10-29.

18. Bird, R.B., Dai, G.C., and Yarusso, B.J.: "The Rheology and Flow of Viscoplastic Materials," *Reviews in Chem. Eng.* (1983) **1**, No.1, 1.
19. Seright, R.S.: "Conformance Improvement Using Gels," Semi-Annual Technical Progress Report, U.S. DOE Contract No. DE-FC26-01BC15316, Washington, DC (March 2003), 47-58.
20. Macosko, C.W.: *Rheology Principles, Measurements, and Applications*, WILEY-VCH, New York City (1994), 97-98, 108-140,.
21. Yoshimura, A. and Prud'homme, R.K.: "Wall Slip Corrections for Couette and Parallel Disk Viscometers," *J. of Rheology* (1988) **32**, No.1, 53.
22. Yoshimura, A. and Prud'homme, R.K.: "Viscosity Measurements in the Presence of Wall Slip in Capillary, Couette, and Parallel-Disk Geometries," *SPEPE* (May 1988) 735.
23. Ganguly, G. *et al.*: "The Effect of Fluid Leakoff on Gel Placement and Gel Stability in Fractures," *SPEJ* (September 2002) 309.
24. Taber, J.J., Martin, F.D., and Seright, R.S.: "EOR Screening Criteria Revisited-Part 1: Introduction to Screening Criteria and Enhanced Recovery Field Projects," *SPEPE* (August 1997) 189.
25. Bird, R.B., Stewart, W.E., and Lightfoot, E.N.: *Transport Phenomena*, John Wiley & Sons, New York (1976) 42-46, 62-63.
26. Seright, R.S.: "Use of Preformed Gels for Conformance Control in Fractured Systems," *SPEPF* (February 1997) 59.
27. Seright, R.S.: "Polymer Gel Dehydration during Extrusion through Fractures," *SPEPF* (May 1999) 110.
28. Broseta, D., Marquer, O., and Zaitoun, A.: "Shear Effects on Polyacrylamide / Chromium (III) Acetate Gelation," paper SPE 50750 presented at the 1999 SPE International Symposium on Oilfield Chemistry, Houston, Texas, 16-19 February.
29. Wang, C.Y., Li, Q.Z., Zheng, J.M., and Guo, C.T.: "Die-swell Measurement for the Evaluation of Elasticity of Mesophase Pitches," *Carbon* (1998) **36**, No.12, 1861.
30. Bigg, D.M.: "Rheology and Wire Coating of High Atomic Number Metal-low Density Polyethylene Composites," *Polymer Eng. Sci.* (1977) **17**, No.10, 745.
31. Liang, J.Z.: "Predictions of Primary Normal Stress Difference from Extrudate Swell of Rubber Compound," *Plastics, Rubber and Composites Processing and Applications* (1996) **25**, No. 5, 257.
32. Magda, J.J., Lee, C-S., Muller, S.J.; and Larson, R.G.: "Rheology, Flow Instabilities, and Shear-induced Diffusion in Polystyrene Solutions," *Macromolecules* (1993) **26**, No. 7, 1696.
33. Lerdwijitjarud, W., Sirivat, A., and Larson, R.G.: "Influence of Dispersed-phase Elasticity on Steady-state Deformation and Breakup of Droplets in Simple Shearing Flow of Immiscible Polymer Blends," *J. of Rheology* (2004) **48**, No. 4, 843.
34. Takahashi, Y. *et al.*: "Experimental Tests of the Scaling Relation for Textured Materials in Mixtures of Two Immiscible Fluids," *J. of Rheology* (1994) **38**, No. 3, 699.
35. Meijer, H.E.H. and Bulters, M.J.H.: "Analogy between the Modeling of Pullout in Solution Spinning and the Prediction of the Vortex Size in Contraction Flows," *Chem. Eng. Research & Design* (1991) **69**, No. 3, 190.
36. Meister, B.J. and Biggs, R.D.: "Prediction of the First Normal Stress Difference in Polymer Solution," *AIChE J* (1969) **15**, No. 5, 643.
37. Fried, F. *et al.*: "First Normal Stress Difference and Viscosity in Shear of Liquid Crystalline Solutions of Hydroxypropyl-cellulose: New Experimental Data and Theory," *Polymer* (1994) **5**, No. 9, 596.
38. Takahashi, Y. *et al.*: "Shear-rate Dependence of First Normal Stress Difference of Poly (isoprene-b-styrene) in Solution near the Order-disorder Transition Temperature," *Polymer* (1996) **37** No. 26, 5943.
39. Vlcek, J., and Bartos, O.: "Use of a Generalized Model Based on the Relaxation Spectrum for Calculation of the First Normal Stress Difference from a Flow Curve," *J. of Non-Newtonian Fluid Mechanics* (1985) **19**, No. 2, 113.

SI Metric Conversion Factors

cp x 1.0*	E-03	= Pa·s
ft x 3.048*	E-01	= m
in. x 2.54*	E+00	= cm
psi x 6.894 757	E+00	= kPa

*Conversion is exact.